# Magnetic Permeability Time-varying Metamaterials at Microwave Frequencies

Toshiyuki Kodama,[1, *] Nobuaki Kikuchi,[2] Takahiro Chiba,[3, 4]
Seigo Ohno,[5] Satoshi Okamoto,[6, 7] and Satoshi Tomita[1, 5, †]

[1] *Institute for Excellence in Higher Education, Tohoku University, Sendai, 980-8576, Japan*
[2] *Department of Electrical and Electronic Engineering,*
*Graduate School of Engineering and Resource Science, Akita University, Akita 010-8502, Japan*
[3] *Frontier Research Institute for Interdisciplinary Sciences, Tohoku University, Sendai 980-8578, Japan*
[4] *Department of Applied Physics, Graduate School of Engineering, Tohoku University, Sendai 980-8579, Japan*
[5] *Department of Physics, Graduate School of Science, Tohoku University, Sendai 980-8578, Japan*
[6] *Institute of Multidisciplinary Research for Advanced Materials, Tohoku University, Sendai 980-8577, Japan*
[7] *Center for Science and Innovation in Spintronics, Tohoku University, Sendai 980-8577, Japan*
(Dated: March 7, 2025)

We demonstrate magnetic permeability ($\mu$) time-varying metamaterials at GHz frequencies using ferromagnetic permalloy ($Ni_{80}Fe_{20}$; Py). We observe frequency up and down conversion of 4 GHz microwaves through the metamaterials, which is caused by the temporal modulation of $\mu$ in the Py layer. Moreover, the efficiency of the up-conversion to a higher frequency is much larger than that of the down conversion to a lower frequency. These experimental results are reproduced well via numerical calculation, verifying that the significant up-conversion efficiency is traced back to non-linear magnetization dynamics in the metamaterials. The present study opens a door to microwave sources toward the 6th-generation mobile communication system, four-dimensional metamaterials with spatio-temporal modulation, and nonlinear spintronics.

*Introduction* – Noether's theorem [1] says that a system with a continuous symmetry has a conserved quantity. In a medium with the space-translational symmetry, the conjugated quantity, wavevector of light, is conserved. When the space-translational symmetry is broken at a spatial boundary between different indices of refraction, for example, at the interface of a prism, the wavevector is not conserved, resulting in refraction of light [2]. Contrastingly, frequency (energy) of light is a conjugated quantity in a medium with the time-translational symmetry. In a time-varying medium with broken time-translation symmetry, therefore, frequencies of light have to change while leaving the wavevector unchanged [3]; this is the principle of frequency conversion using an electro-optic (EO) modulator toward optical frequency-comb in modern optics [4, 5]. This principle is applicable in man-made structured materials, metamaterials, exhibiting exotic optical properties unavailable in natural materials.

The most typical metamaterials are metamaterials with a negative index of refraction [6] and for invisible cloaks [7]. These are referred to as space-varying metamaterials because the wavevectors of light are changed at the spatial boundary. Recently, a new paradigm for light generation and steering has emerged [8] – time-varying metamaterials, in which refractive indices are temporally modulated. Time-varying metamaterials would bring about promising applications to frequency converters [9, 10, 14], nonreciprocal devices [11], and anti-reflection temporal coatings [12, 13] as well as exotic phenomena, for example, time refraction [14] and reflection [15, 16], analogue of a continuous time crystal [17], and temporal aiming [18].

The temporal modulation of refractive indices has been achieved experimentally using time modulated electric permittivity ($\varepsilon$) [3, 14]. However, time modulation of magnetic permeability ($\mu$) is expected because $\mu$ is the counterpart of $\varepsilon$ in the refractive index $n = \sqrt{\varepsilon}\sqrt{\mu}$. The space-time modulation of both $\varepsilon$ and $\mu$ is essential for investigating Fresnel drag for light in optically moving media [19], spatio-temporal four-dimensional control of wave-matter interactions [20], quantum electrodynamics phenomena [21–23], and Doppler cloaks [24]. In any cases, the key is the realization of $\mu$ time-varying metamaterials. Nevertheless, experimental demonstration of time modulation of $\mu$ is lacking.

In an electrical circuit analogue, $\mu$ modulation is regarded as an inductance variation. As inductance is relevant to turn numbers, length, and cross section of coils, time-varying $\mu$ intuitively seems to be a tough challenge. However, $\mu$ can be varied in magnetic materials. In particular, ferromagnetic materials show frequency dispersion of $\mu$ in the vicinity of ferromagnetic resonance (FMR) frequencies in the microwave region. Furthermore, a large magnetization originated from coupled microscopic electron spins in the ferromagnets gives rise to a large variation in $\mu$. In this way, $\mu$ time-varying metamaterials at GHz frequencies are realized when the FMR conditions are temporally modulated. Although several possibilities using spintronic techniques are proposed [25, 26], an important issue to be addressed is how the effective magnetic fields for FMR are dynamically changed at high frequencies.

In this Letter, we prepare magnetic metamaterials including a ferromagnetic-metal (permalloy (Py), $Ni_{80}Fe_{20}$) layer, together with microwave carrier and
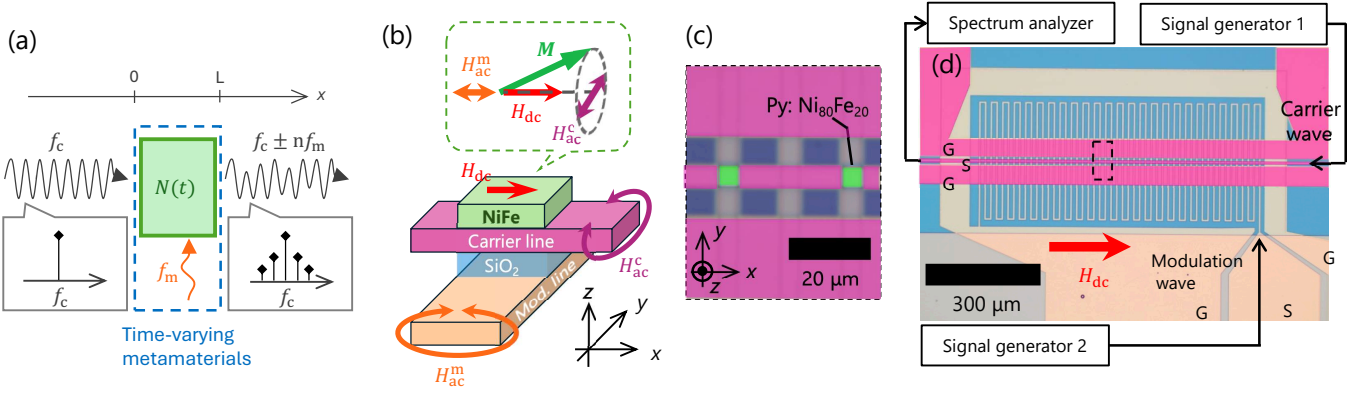
FIG. 1. (a) Schematic illustration of frequency conversion by a time-varying metamaterial with a refractive index $N(t)$ and a modulation frequency $f_m$. A frequency of a carrier wave to be modulated is $f_c$. (b) Bottom: schematic illustration of the metamaterial structures. Top: configurations of magnetization ($M$) in precession and magnetic fields ($H$) for excitation and modulation of FMR. (c) Enlarged optical microscope image of the metamaterial. (d) Overview photo of the metamaterial together with illustration of measurement setup. The enclosed area by the black dashed line corresponds to (c).

modulation lines. While the microwaves in the carrier line excites FMR in the Py layer, a time-periodic Oersted magnetic field generated by another microwave in the modulation line alters the effective magnetic field for FMR temporally at GHz frequencies. We observe frequency conversion of the carrier microwaves and verify that the conversion is caused by the temporal modulation of $\mu$ in the Py layer on FMR. A magnetic counterpart of the EO modulator is realized at microwave frequencies. The most striking feature of the $\mu$ time-varying metamaterial is that the up-conversion efficiency is much larger than the down-conversion efficiency. This would be advantageous to study Floquet engineering of light-matter interaction [27, 28] and realize microwave/millimeter-wave sources toward the 6th-generation mobile communication system.

The experimental results are reproduced well via numerical calculation, indicating that the significant up-conversion efficiency is traced back to nonlinear magnetization dynamics in the $\mu$ time-varying metamaterials. Although nonlinear magnetization dynamics and microwave response through nonlinear susceptibility have attracted much attention in spintronics [29, 30], the physical mechanism is still unclear. The present study is thus an important step for further investigation in the nonlinear magnonics [31]. Furthermore, as the present temporally $\mu$ modulated metamaterials are prepared on microwave circuits, it can be easily integrated with $\varepsilon$-modulated metamaterials. Therefore, the present study paves a way for space-time modulation of both $\varepsilon$ and $\mu$ in metamaterials, opening a door for experimental demonstration of relativistic and quantum effects in spatio-temporal four-dimensional metamaterials [19–23].

*Principle of frequency conversion by permeability modulation* – Figure 1(a) shows a schematic illustration of frequency conversion by a time-varying metamaterial.

Suppose a one-dimensional propagation of a carrier wave having a frequency of $f_c$ into the $x$ direction. The carrier wave is injected to a medium with a time-dependent complex refractive index $N(t) = n(t) - j\kappa(t)$, which is modulated in time by a modulation wave having a frequency of $f_m$. The length of the medium $L$ is much smaller than the carrier wavelength. The plane wave's magnetic field at time $t$ and position $L$ in the medium, $H(t, x = L)$, is expressed as

$$H(t, x = L) = H_0 \exp[2\pi j(f_c t - \frac{N(t)f_c}{c}L)], \quad (1a)$$

$$= H_0 \exp(-2\pi \frac{\kappa(t)f_c}{c}L)\exp[2\pi j(f_c t - \frac{n(t)f_c}{c}L)], \quad (1b)$$

where $H_0$ is an amplitude of the carrier wave and $c$ is the speed of light in vacuum. Equation (1b) indicates that the first exponential term containing $\kappa(t)$ corresponds to amplitude modulation. Contrastingly, the second exponential term including $n(t)$ represents phase modulation. When $n(t)$ is varied periodically as $\sin(\omega t)$, this term is described using the Vessel's function. The carrier wave frequency is thus converted as $f_c \pm n f_m$ with $n = 1, 2, \cdots$. Note that even if the medium originally shows a linear response, for example, FMR in a ferromagnetic material, an energy injected by the modulation wave with $f_m$ causes nonlinear processes, resulting in frequency conversions of the carrier waves. In this way, a linear medium with the applied modulation power, surrounded by blue dashed lines in Fig. 1(a), is regarded as the time-varying metamaterial.

Time modulated $N(t)$ can be realized through $\varepsilon(t)$ and $\mu(t)$. In this study, $\mu(t)$ is achieved using ferromagnetic metamaterials. The bottom part of Fig. 1(b) illustrates the structure of the $\mu(t)$ metamaterial's unit cell. The metamaterial consists of four layers: a ferromagnetic Py

top layer (green) with magnetization ($M$) under dc magnetic field $H_{dc}$, a gold (Au) carrier line (red) for FMR excitation by ac magnetic field $H_{ac}^c$, a silicon dioxide (SiO$_2$) spacer (blue), and an Au modulation line (orange) for generating ac magnetic field $H_{ac}^m$ to periodically change the FMR condition and vary the permeability of Py.

The upper panel of Fig. 1(b) presents the configuration of magnetization $M$ and magnetic fields $H$ in the Py layer. The carrier microwave current with a frequency of $f_c$ injected into the carrier microstrip line generates an ac Oersted magnetic field $H_{ac}^c(t)$ by the Ampère's law. Under $H_{dc}$, the ac Oersted field $H_{ac}^c$, which is along the $y$-axis and perpendicular to $H_{dc}$, drives precession of in-plane $M$ in the Py layer (FMR). The FMR condition is described by the Kittel's equation for thin magnetic films as

$$2\pi f_{FMR} = \gamma\sqrt{\mu_0 H_{ext}(\mu_0 H_{ext} + \mu_0 M_{eff})}. \qquad (2)$$

The FMR frequency $f_{FMR}$ is determined by the gyromagnetic ratio $\gamma$, the effective magnetic fields along precession axis $H_{ext}$, the effective magnetization $M_{eff}$, and magnetic permeability of vacuum $\mu_0$.

The modulation microwave current with a frequency of $f_m$ generates another ac Oersted magnetic field $H_{ac}^m(t)$ around the modulation microstrip lines. As in Fig. 1(b), $H_{ac}^m$ oscillating in $f_m$ is parallel to $H_{dc}$ so that the effective magnetic fields for FMR ($H_{ext}$) is expressed as $H_{ext}(t) = H_{dc} + H_{ac}^m(t)$. In this way, time modulation of $H_{ext}$ with the frequency of $f_m$ results in dynamic change in $f_{FMR}$.

The relative permeability $\mu_r$ of the Py layer on FMR shows frequency dispersion at the vicinity of $f_{FMR}$. The real $\mu_r'$ and imaginary $\mu_r''$ parts of $\mu_r$ at the carrier wave frequency $f_c$ are written as [26]

$$\mu_r' = 1 + \frac{\gamma\mu_0 M_{eff}}{2\pi}\frac{f_{FMR}(f_{FMR}^2 - f_c^2) + f_{FMR}f_c^2\alpha^2}{[f_{FMR}^2 - f_c^2(1+\alpha^2)]^2 + 4f_{FMR}^2 f_c^2\alpha^2}, \qquad (3a)$$

$$\mu_r'' = \frac{\gamma\mu_0 M_{eff}}{2\pi}\frac{\alpha f[f_{FMR}^2 - f_c^2(1+\alpha^2)]}{[f_{FMR}^2 - f_c^2(1+\alpha^2)]^2 + 4f_{FMR}^2 f_c^2\alpha^2}, \qquad (3b)$$

where $\alpha$ is the Gilbert damping parameter. Equations (3a) and (3b) indicate that, when $f_{FMR}$ is dynamically changed in time with the frequency of $f_m$, the time modulation of $\mu_r'$ and $\mu_r''$ is plausible.

*Experimental procedures* – Figures 1(c) and 1(d) present optical microscopy images of the metamaterial consisting of arrays of the unit cell illustrated in Fig. 1(b). Fig. 1(c) corresponds to the area enclosed by the black dashed line in Fig. 1(d). The metamaterial is prepared by thin films deposition on an undoped silicon substrate using Ar-ion magnetron sputtering at room temperature followed by microfabrication using photolithography and lift-off techniques. Figure 1(c) shows that the

vertical Au modulation lines (orange) have width of 5 µm and spacing of 10 µm. The modulation line is prepared as a meandering track repeated 25 times, of which the total length is 16 mm, as shown in Fig. 1(d). The Au thickness of the modulation line is 200 nm. An SiO$_2$ layer (blue) of 200 nm thickness is deposited followed by the deposition of another Au layer and patterning of the horizontal carrier line (red). The carrier line is patterned as a coplanar waveguide (CPW) consisting of a 5 µm-width signal line (S) sandwiched between two 50 µm-width ground lines (G). The gap between S and G lines is 5 µm. Eventually, a 5-nm-thick tantalum (Ta) layer followed by a 250-nm-thick Py layer are deposited at the $5 \times 5$ µm intersection area (green) of the modulation and carrier lines. Because the current flows in the opposite direction between the adjacent modulation lines, the Ta/Py layers are formed at every other intersection as shown in the Fig. 1(c). The total number of the unit cell is 25 so that the total length of the metamaterial is 725 µm.

Figure 1(d) illustrates the measurement setup. A dc magnetic field $\mu_0 H_{dc}$ in a range of +70 mT to −70 mT is applied along the $x$-axis using an electromagnet. One side of the CPW is connected to a signal generator via a 10 dBm attenuator for the carrier microwave current injection. The signal generator power is set to 18 dBm so that the actual power for FMR excitation is 8 dBm, corresponding to $P_c = 6.31$ mW if a resister of 50 Ω is connected instead of the CPW. The carrier wave with $P_c = 6.31$ mW generates the amplitude of $H_{ac}^c$ to be 1.15 mT at the Py patch. (See Fig. S1 in Supplemental Materials [32]). The injected carrier wave frequency $f_c$ is fixed at 4.0 GHz. The wavelength of the carrier waves in vacuum (75 mm) is much larger than the length of the unit cell (5 µm) and the metamaterial (725 µm). The metamaterial is thus excited uniformly by the carrier waves.

The spectra of transmitted carrier waves are measured using a spectrum analyzer via a 10 dBm attenuator. The signals measured by the spectrum analyzer are averaged by $10^4$ times. The settings of the spectrum analyzer are as follows: the center frequency of 4.0 GHz, the measurement span of 4.0 GHz, the number of data points of 20001, and the resolution bandwidth of 3 MHz. Another signal generator for temporal modulation is connected to the meandering modulation line. Microwaves with $f_m$ and 20 dBm, corresponding to $P_m = 100$ mW, are injected into the modulation line. The evaluated $H_{ac}^m$ of the 100 mW modulation waves is 4.6 mT at the Py patch. (See Fig. S1 in Supplemental Materials [32]). The modulation frequency $f_m$ is varied from 0.1 GHz to 1.8 GHz.

*Experimental results* – Figure 2 shows spectra of the transmitted microwaves of $f_c = 4.0$ GHz at various $f_m$ under $\mu_0 H_{dc} = 24.4$ mT. The vertical axis represents the microwave power. The most powerful signal at 4.0 GHz is an unmodulated carrier wave. When $f_m = 0.1$ GHz (purple), two signals are observed besides the 4.0 GHz carrier
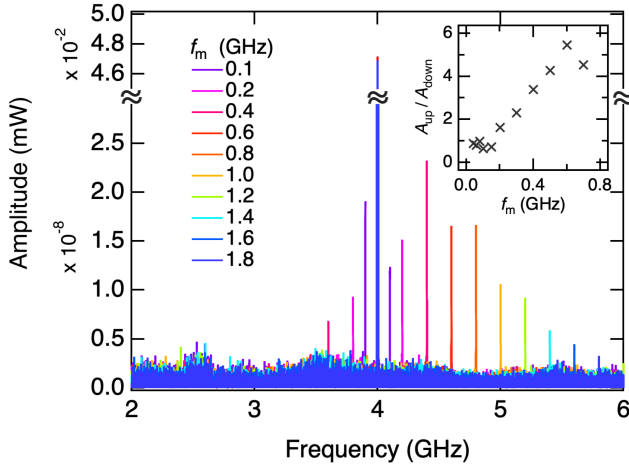
FIG. 2. Output microwaves spectra of $f_c = 4.0$ GHz under $\mu_0 H_{dc} = 24.4$ mT at various modulation frequency $f_m$ in the range from 0.1 GHz to 1.8 GHz. Inset: peak amplitude ratio $A_{up}/A_{down}$ is plotted as a function of $f_m$.
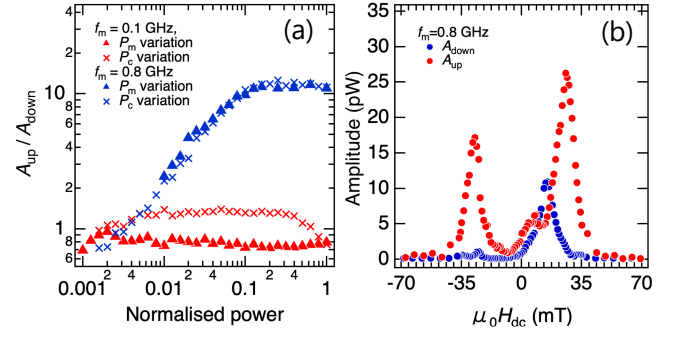


FIG. 3. (a) Peak amplitude ratios of up-conversion to down-conversion signals $A_{up}/A_{down}$ at $\mu_0 H_{dc} = 24.4$ mT are plotted as a function of normalized modulation power $P_m/(100\,\text{mW})$ (triangles) and carrier power $P_c/(6.31\,\text{mW})$ (crosses). Red and blue correspond to $f_m = 0.1$ GHz and $f_m = 0.8$ GHz, respectively. (b) $A_{down}$ at 3.2 GHz (blue) and $A_{up}$ at 4.8 GHz (red) with $f_m = 0.8$ GHz are plotted as a function of $\mu_0 H_{dc}$.

microwave with a spacing of $f_m = 0.1$ GHz: signals at a lower frequency of 3.9 GHz and at a higher frequency of 4.1 GHz, corresponding to down- and up-converted waves of the $f_m = 4.0$ GHz carrier wave, respectively. The frequencies of the converted waves are expressed as $4.0 \pm f_m$ GHz. At $f_m$ up to 0.4 GHz (pink), both the down- and up-converted waves are observed in Fig. 2. The down-converted wave at $f_m = 0.6$ GHz (orange) is detectable but the intensity is comparable to the noise. At above $f_m = 0.8$ GHz (red), the down-converted wave cannot be detected.

Note that Fig. 2 presents only the first-order converted signals. However, the second-order converted signals expressed as $f_c \pm 2f_m$ are observed in high sensitivity measurements with the measurement span of 1 MHz, number of data points of 2001, and resolution bandwidth of 9.1 kHz. Indeed in Fig. S2 in Supplemental Materials [32], high sensitivity measurements with $f_c = 4.0$ GHz and $f_m = 0.1$ GHz demonstrate the $f_c \pm 2f_m$ signals at 3.8 and 4.2 GHz although the signal intensities are very small.

Figure 2 presents that, at $f_m = 0.1$ GHz, the peak amplitude of the down conversion signal $A_{down}$ is larger than that of the up conversion signal $A_{up}$. However, $A_{up}$ becomes more intensive than $A_{down}$ as $f_m$ increases from 0.2 to 1.8 GHz. This is remarkable because the $A_{down}$ and $A_{up}$ should be the same according to Eq. (1). In the inset of Fig. 2, the amplitude ratio $A_{up}/A_{down}$ is plotted as a function of $f_m$ from 0.04 to 0.7 GHz. Whereas $A_{up}$ is slightly smaller than $A_{down}$ at $f_m \leq 0.18$ GHz, $A_{up}$ becomes larger than $A_{down}$ at $f_m \geq 0.2$ GHz. Furthermore, as $f_m$ increases, $A_{up}/A_{down}$ increases monotonically; eventually at $f_m = 0.6$ GHz, $A_{up}$ is 5.5 times larger than $A_{down}$.

The dependence of $A_{up}/A_{down}$ on modulation power $P_m$ and carrier power $P_c$ is studied in high sensitiv-

ity measurements as $P_m$ or $P_c$ decreases. Triangles in Fig. 3(a) present $A_{up}/A_{down}$ at $\mu_0 H_{dc} = 24.4$ mT as a function of normalized modulation power $P_m/(100\,\text{mW})$. When $f_m = 0.1$ GHz (red triangles), $A_{up}/A_{down}$ is approximately 1 and is independent of $P_m$. In contrast, when $f_m = 0.8$ GHz (blue triangles), $A_{up}/A_{down}$ remains constant at 10 as $P_m/(100\,\text{mW})$ decreases to 0.2, and $A_{up}/A_{down}$ decreases monotonically as $P_m/(100\text{mW})$ further decreases to 0.002. Crosses in Fig. 3(a) highlight dependence of $A_{up}/A_{down}$ on the normalized carrier power $P_c/(6.31\,\text{mW})$. At $f_m = 0.1$ GHz (red crosses) and $f_m = 0.8$ GHz (blue crosses), $A_{up}/A_{down}$ depends on $P_c$ in a similar way with $P_m$. Given that the vertical and horizontal axes of Fig. 3(a) are logarithmic scales, $A_{up}/A_{down}$ at $f_m = 0.8$ GHz (blue) shows nonlinear response to $P_m$ and $P_c$.

In Fig. 3(b), when $f_c = 4.0$ GHz and $f_m = 0.8$ GHz, $A_{up}$ at 4.8 GHz (red circles) and $A_{down}$ at 3.2 GHz (blue circles) are plotted as a function of $\mu_0 H_{dc}$ from $+70$ to $-70$ mT. As $\mu_0 H_{dc}$ decreases from $+70$ mT, both $A_{up}$ and $A_{down}$ increase. While $A_{up}$ reaches the maximum at $\mu_0 H_{dc} = 25.7$ mT, $A_{down}$ reaches the maximum at $\mu_0 H_{dc} = 15.2$ mT. These magnetic fields for the maximum amplitude are consistent with the Kittel's FMR condition. (See Fig. S3(c) in Supplemental Materials [32] in more detail.) With a further decrease in $\mu_0 H_{dc}$ to 0 mT, the amplitude $A_{up}$ and $A_{down}$ decreases to zero. In the $\mu_0 H_{dc} < 0$ region, $A_{down}$ at 3.2 GHz reaches the maximum at $\mu_0 H_{dc} = -25.2$ mT, while $A_{up}$ at 4.8 GHz shows the maximum at $\mu_0 H_{dc} = -27.2$ mT. Furthermore, the amplitude difference between $A_{up}$ at $\mu_0 H_{dc} > 0$ and $A_{up}$ at $\mu_0 H_{dc} < 0$ is traced back to the magnetization hysteresis on vortex states [33]. (See Fig. S4 in Supplemental Materials [32]).

*Theoretical consideration* – To shed light on the physical origin of the asymmetric frequency conversion ef-
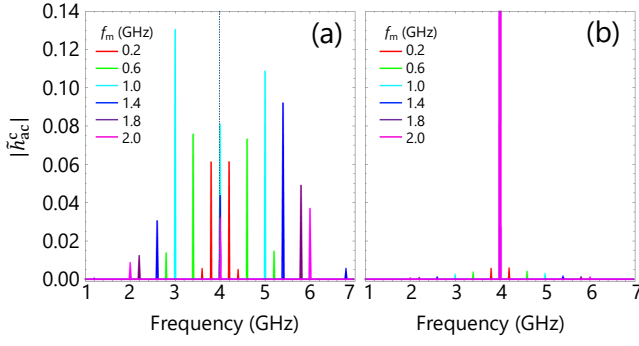
FIG. 4. Calculation results of microwave magnetic field $\tilde{h}_{\text{ac}}^{\text{c}}$ (a) with and (b) without the demagnetization field arising from the shape anisotropy. While $f_{\text{c}}$=4.0 GHz is fixed as indicated by the vertical dashed line, $f_{\text{m}}$ is varied from 0.2 GHz to 2.0 GHz.

ficiency, we theoretically consider a forced oscillation model based on the Maxwell's equation for electromagnetic waves combined with the Landau-Lifshitz-Gilbert equation for magnetization precession. In the model, a microwave magnetic field is weakly coupled to the magnetization dynamics of the magnetic material. See the calculation details in Supplemental Material [32] and references [34, 35] therein. As an initial condition, an FMR excitation field of 4.0 GHz with an amplitude of 4.6 mT and an ac modulation field of $f_{\text{m}}$ with an amplitude of 1.15 mT are considered. The dc magnetic field $\mu_0 H_{\text{dc}}$ is 25 mT. The magnetization precession is driven at 4.0 GHz and modulated at $f_{\text{m}}$. $f_{\text{m}}$ is varied from 0.2 GHz to 2.0 GHz. The microwave magnetic field $\tilde{h}_{\text{ac}}^{\text{c}}$ is calculated in the time domain. The time-axis waveforms of $\tilde{h}_{\text{ac}}^{\text{c}}$ are Fourier transformed to the spectra.

Figure 4(a) presents the calculated spectra of $|\tilde{h}_{\text{ac}}^{\text{c}}|$ affected by a demagnetization field of the thin film shape of Py. Up- and down-converted signals at $f_{\text{c}} \pm f_{\text{m}}$ is reproduced well in the numerical calculation. At $f_{\text{m}} = 0.2$ GHz (red) and 0.6 GHz (green), amplitudes of $|\tilde{h}_{\text{ac}}^{\text{c}}|$ of the up- and down-converted signals are similar. Note that the second-order converted signals are observed at 4.0 $\pm 2 f_{\text{m}}$ GHz in Fig. 4(a). At $f_{\text{m}} = 1.0$ GHz (light blue), $|\tilde{h}_{\text{ac}}^{\text{c}}|$ of the up-conversion signal is slightly smaller than that of the down-conversion signal. However, when $f_{\text{m}}$ is further increased to 1.4 GHz (blue), 1.8 GHz (purple), and 2.0 GHz (magenta), $|\tilde{h}_{\text{ac}}^{\text{c}}|$ of the up-conversion signal becomes significantly larger than that of the down-conversion signal. The relative $|\tilde{h}_{\text{ac}}^{\text{c}}|$ reproduces qualitatively experimental results observed in the inset of Fig. 2. The quantitative discrepancy between the calculation and experimental results is probably originated from the magnetic dipole interactions of a micron-scale sample, which are not taken into account in our macrospin mode.

Figure 4(b) shows calculation results of a model without demagnetization field. When the demagnetization field is zero, corresponding to the Py sphere, $|\tilde{h}_{\text{ac}}^{\text{c}}|$ of con-

verted signals decrease drastically in Fig. 4(b). Moreover, at $f_{\text{m}} = 2.0$ GHz, $A_{\text{up}}/A_{\text{down}}$ of 4.45 in Fig. 4(a) decrease to 1.63 in Fig. 4(b). Therefore, the demagnetization field due to the magnetic shape anisotropy causes nonlinear magnetization dynamics [31], giving rise to asymmetrical frequency conversions.

*Discussion* – In Fig. 3(b), $A_{\text{up}}$ and $A_{\text{down}}$ as a function of $\mu_0 H_{\text{dc}}$ highlights that no conversion is observed at $\mu_0 H_{\text{dc}} = 0$ and $\pm$ 70 mT. Moreover, up- and down-conversion efficiency shows maximum value when $\mu_0 H_{\text{dc}}$ is in FMR condition of each converted wave. These results clearly indicate that the frequency conversion is caused by the time modulation in $\mu$ of Py on FMR. In this way, we have demonstrated $\mu$ time-varying metamaterials at microwave frequencies.

The most striking feature in the microwave frequency conversion by the $\mu$ time-varying metamaterials is that the up-conversion efficiency is increased in a nonlinear fashion and much larger than the down-conversion efficiency particularly at larger $f_{\text{m}}$ as shown experimentally in Fig. 2 and numerically in Fig. 4. Experimentally at $f_{\text{m}} = 0.6$ GHz, $A_{\text{up}}$ is 5.5 times larger than $A_{\text{down}}$. Equations (1a) and (1b) under moderate modulation fields do not predict such asymmetric conversion. Therefore, the significant up-conversion is caused by intensive modulation fields with high modulation frequency. This would be advantageous for realizing microwave/millimeter-wave sources toward the 6th-generation mobile communication system.

It is reported [36] that electron-hole pairs (excitons) created by weak near-infrared laser in semiconductor quantum wells is strongly modulated by intensive electric fields by a THz free electron laser, resulting in asymmetric modulation with much larger conversion efficiency at higher frequency. The study in the electric counterpart consider microscopic nonlinear dynamics of exciton under intensive electric fields. Similarly in this study, we consider nonlinear dynamics of spin waves (magnons) created by carrier microwaves in the Py layer, which are strongly modulated by intensive magnetic fields of the modulation microwaves. Fig. 3(a) reveals that the conversion ratio depends on the power of the carrier and modulation microwaves, indicating a nonlinear process by the intense magnetic fields in the asymmetric conversion. Numerical simulation in Fig. 4 demonstrates that the nonlinear magnetization dynamics due to the demagnetization field is essential to the asymmetrical conversion. Analogous to the frequency conversion in nonlinear optics, asymmetrical frequency conversions using $\mu$ time-varying metamaterials is traced back to the a higher order magnetic susceptibility through nonlinear magnetization dynamics, for example, $\chi^{(3)}$ and nonlinear $\mu$. The frequency dependence of nonlinear $\mu$ results in the asymmetric frequency conversion efficiency.

Last but not least, the present metamaterial is based on the microwave circuit so that integration with $\varepsilon$

time-modulation systems are feasible using EO modulators or micro electro-mechanical systems (MEMS) [37]. This paves a way to investigate spatio-temporal four-dimensional control of light and the relativistic phenomena in solid state. Although nonlinear magnetization dynamics and microwave response through nonlinear susceptibility have attracted attention in spintronics [29, 30], the physical mechanism is still unclear. The present study is thus an important step in the nonlinear spintronics. Furthermore, as the $\mu$ time-varying metamaterial is regarded as a weakly coupled magnon-photon coupling system in the theoretical consideration, the present study leads to nonlinear phenomena in magnon-polaritons [35].

*Conclusion* – We demonstrate magnetic $\mu$ time-varying metamaterials at GHz frequencies using ferromagnetic Py. FMR in the Py thin film excited by the carrier microwaves is temporally modulated by oscillating Oersted magnetic fields of another microwave. We observe frequency up-and-down conversion of the carrier microwaves and verify that the conversion is caused by the temporal modulation of $\mu$ in the Py layer. Moreover at $f_\mathrm{m} = 0.6$ GHz, $A_\mathrm{up}$ is 5.5 times larger than $A_\mathrm{down}$. These experimental results are reproduced well via numerical calculation, indicating that the significant up-conversion efficiency is traced back to nonlinear magnetization dynamics due to demagnetization fields in the $\mu$ time-varying metamaterials. The present study paves a way to development of microwave / millimeter-wave sources toward the 6th-generation mobile communication system, realization of space-time modulation of both $\varepsilon$ and $\mu$ in metamaterials for experimental demonstration of relativistic and quantum effects, and further investigation in the nonlinear spintronics and the magnon-photon coupling systems.

---

* Email address:tkodama@tohoku.ac.jp
† Email address:tomita@tohoku.ac.jp

[1] Y. Kosmann-Schwarzbach, B. E. Schwarzbach , *The Noether Theorems: Invariance and Conservation Laws in the Twentieth Century* (Springer, New York, 2011).

[2] E. Hecht, *Optics* (Pearson Education Limited, Harlow, 2013).

[3] F. Miyamaru et al., Ultrafast Frequency-Shift Dynamics at Temporal Boundary Induced by Structural-Dispersion Switching of Waveguides, Phys. Rev. Lett. **127**, 053902 (2021).

[4] T. Udem, R. Holzwarth, T. Hänsch, Nature **416**, 233 (2002).

[5] A. Ishizawa, T. Nishikawa, K. Hitachi, T. Akatsuka, K. Oguri, Sci. Rep. **13**, 8750 (2023).

[6] R. A. Shelby, D. R. Smith, and S. Schultz, Experimental verification of a negative index of refraction, Science **292**, 77 (2001).

[7] D. Schurig, J. J. Mock, B. J. Justice, S. A. Cummer, J. B. Pendry, A. F. Starr, and D. R. Smith, Metamaterial electromagnetic cloak at microwave frequencies, Science **314**, 977 (2006).

[8] E. Galiffi, R. Tirole, S. Yin, H. Li, S. Vezzoli, P. A. Huidobro, M. G. Silveirinha, R. Sapienza, A. Alú, and J. B. Pendry, Photonics of time-varying media, Advanced Photonics **4**, 0140022 (2022).

[9] L. P. Zhang, H. C. Zhang, J. Zhang, L. Y. Niu, P. H. He, C. Wei, W. Tang, and T. J. Cui, Reprogrammable control of electromagnetic spectra based on time-coding plasmonic metamaterials, Appl. Phys. Lett. **121**, 161702 (2022).

[10] S. Taravati and G. V. Eleftheriades, Pure and Linear Frequency-Conversion Temporal Metasurface, Phys. Rev. Appl. **15**, 064011 (2021).

[11] X. Guo, Y. Ding, Y. Duan, and X. Ni, Nonreciprocal metasurface with space-time phase modulation, Light Sci. Appl. **8**, (2019).

[12] V. Pacheco-Peña and N. Engheta, Antireflection temporal coatings, Optica **7**, 323 (2020).

[13] I. Liberal, J. E. Vázquez-Lozano, and V. Pacheco-Peña, Quantum antireflection temporal coatings: Quantum state frequency shifting and inhibited thermal noise amplification, Laser Photon. Rev. **17**, (2023).

[14] Y. Zhou, M. Z. Alam, M. Karimi, J. Upham, O. Reshef, C. Liu, A. E. Willner, and R. W. Boyd, Broadband frequency translation through time refraction in an epsilon-near-zero material, Nat. Commun. **11**, 1 (2020).

[15] B. Apffel and E. Fort, Frequency Conversion Cascade by Crossing Multiple Space and Time Interfaces, Phys. Rev. Lett. **128**, 064501 (2022).

[16] H. Moussa, G. Xu, S. Yin, E. Galiffi, Y. Ra'di, and A. Alú, Observation of temporal reflection and broadband frequency translation at photonic time interfaces, Nat. Phys. **1** (2023).

[17] T. Liu, J.-Y. Ou, K. F. MacDonald, and N. I. Zheludev, Photonic metamaterial analogue of a continuous time crystal, Nat. Phys. **19**, 986 (2023).

[18] V. Pacheco-Peña and N. Engheta, Temporal aiming, Light Sci. Appl. **9**, 129 (2020).

[19] P. A. Huidobro, E. Galiffi, S. Guenneau, R. V. Craster, and J. B. Pendry, Fresnel drag in space-time-modulated metamaterials, Proc. Natl. Acad. Sci. USA **116**, 24943 (2019).

[20] N. Engheta, Four-dimensional optics using time-varying metamaterials, Science **379**, 1190 (2023).

[21] W. J. M. Kort-Kamp, A. K. Azad, and D. A. R. Dalvit, Space-time quantum metasurfaces, Phys. Rev. Lett. **127**, 043603 (2021).

[22] J. Pendry and S. A. Horsley, QED in space-time varying materials, APL Quantum **1**, (2024).

[23] M. G. Silveirinha, Hawking-type radiation in transluminal gratings, Proc. Natl. Acad. Sci. U. S. A. **120**, e2313369120 (2023).

[24] B. Liu, H. Giddens, Y. Li, Y. He, S.-W. Wong, and Y. Hao, Design and experimental demonstration of Doppler cloak from spatiotemporally modulated metamaterials based on rotational Doppler effect, Opt. Express **28**, 3745 (2020).

[25] T. Kodama, N. Kikuchi,S. Okamoto, S. Ohno, and S. Tomita, Spin-current Driven Permeability Variation for Time-varying Magnetic Metamaterials, Phys. Rev. Appl. **19**, 044080 (2023).

[26] T. Kodama, N. Kikuchi, T. Chiba, S. Okamoto, S. Ohno, and S. Tomita, Direct observation of current-induced nonlinear spin torque in Pt-Py bilayers, Phys. Rev. B. **109**, 214419 (2024).

[27] T. Oka and S. Kitamura, Floquet Engineering of Quantum Materials, Annu. Rev. Condens. Matter Phys. **10**, 387 (2019).

[28] S. Yin, E. Galiffi, and A. Alú, Floquet metamaterials, eLight **2**, 8 (2022).

[29] R. Sharma, N. Sisodia, E. Iacocca, A. A. Awad, J. Åkerman, and P. K. Muduli, A high-speed single side-band generator using a magnetic tunnel junction spin torque nano-oscillator, Sci. Rep. **7**, 13422 (2017).

[30] J. Wu, J. Liu, Z. Ren, M. Y. Leung, W. K. Leung, K. O. Ho, X. Wang, Q. Shao, and S. Yang, Wideband coherent microwave conversion via magnon nonlinearity in a hybrid quantum system, Npj Spintronics **2**, 1 (2024).

[31] S. Zheng, Z. Wang, Y. Wang, F. Sun, Q. He, P. Yan, H. Y. Yuan, Tutorial: Nonlinear magnonics, J. Appl. Phys. **134**, 151101 (2023).

[32] See Supplemental Materials at URL for Oersted fields on microstrip lines, experimentally obtained higher-order converted waves, co-planar waveguide FMR measurement, hysteresis feature of converted waves, and Details of theoretical model.

[33] T. Wurft, W. Raberg, K. Prügl, A. Satz, G. Reiss, and H. Brückl, Evolution of magnetic vortex formation in micron-sized disks, Appl. Phys. Lett. **115**, 132407 (2019).

[34] T. Chiba, T. Komine, and T. Aono, Ultrastrong-coupled magnon-polariton in a dynamical inductor based on magnetic-insulator/topological-insulator bilayers, Appl. Phys. Lett. **124**, 012402 (2024).

[35] K. Mita, T. Chiba, T. Kodama, T. Ueda, T. Nakanishi, K. Sawada, and S. Tomita, Ultrastrongly coupled and directionally nonreciprocal magnon polaritons in magnetochiral metamolecules, Phys. Rev. Applied **23**, L011004 (2025).

[36] B. Zaks, R. B. Liu, and M. S. Sherwin, Experimental observation of electron-hole recollisions, Nature **483**, 580 (2012)

[37] Y. Huang, K. Nakamura, Y. Takida, H. Minamide, K. Hane, and Y. Kanamori, Actively tunable THz filter based on an electromagnetically induced transparency analog hybridized with a MEMS metamaterial, Sci. Rep. **10**, 20807 (2020).